J|A|C|S
ARTICLES

# Carboxylic Acid Chemistry at the Ge(100)-2 × 1 Interface: Bidentate Bridging Structure Formation on a Semiconductor Surface

Michael A. Filler, James A. Van Deventer, Albert J. Keung, and Stacey F. Bent*

*Contribution from the Department of Chemical Engineering, Stanford University, Stanford, California 94305*

Received July 22, 2005; E-mail: sbent@stanford.edu

***Abstract:*** The reactions of acetic acid, acetic-$d_3$ acid-*d*, and formic acid with the Ge(100)-2 × 1 surface have been investigated using multiple internal reflection Fourier transform infrared (MIR−FTIR) spectroscopy, X-ray photoelectron spectroscopy (XPS), and density functional theory (DFT) calculations. The infrared and photoelectron data provide experimental evidence for an O−H dissociation product at 310 K. DFT calculations indicate that the O−H dissociation pathway is significantly favored, both kinetically and thermodynamically, over other potential reaction pathways. All of the carboxylic acids studied exhibit unexpected vibrational modes between 1400 and 1525 cm$^{-1}$, which are attributed to the presence of a bidentate bridging structure where both oxygen atoms interact directly with the surface.

## I. Introduction

The organic functionalization of group IV semiconductor surfaces has received significant attention over the past few years due to potential applications in a number of fields, including molecular electronics, nanoscale lithography, and biosensors.[1−5] A large body of work has focused on the kinetics and thermodynamics that govern the reactions of organics with semiconductor surfaces.[6−8] Previous experimental and theoretical studies of organics on UHV-prepared Si(100)-2 × 1 and Ge(100)-2 × 1 surfaces illustrate the high reactivity of these surfaces toward many organic functional groups. In many systems, small activation barriers lead to a distribution of surface products for multifunctional molecules, especially on Si(100)-2 × 1.[9−13] However, Wang and co-workers argue that greater surface product selectivity can be achieved on Ge(100)-2 × 1 due to the desorption of more weakly bound surface products and the larger energy differences between activation barriers of competing reactions.[14] In the current work, we continue to examine the claim of high selectivity put forth by Wang et al. by investigating the reaction of carboxylic acid derivatives on Ge(100)-2 × 1.

The chemistry that occurs on Ge(100)-2 × 1 is largely determined by the unique character of the key active site on group IV (100)-2 × 1 reconstructed surfaces, the surface dimer. Upon proper preparation, the (100) crystal face reconstructs, resulting in surface dimers that possess a strong $\sigma$ bond and weak $\pi$ bond. The energy of the $\pi$ bond has previously been calculated to be approximately 5−6 kcal/mol.[15,16] Past experimental and theoretical findings indicate that Ge dimers are statically tilted at room temperature,[17,18] although recent scanning tunneling microscopy studies of extremely clean and defect-free surfaces find regions of symmetric dimers, as well.[19] Similar to the case of Si(100)-2 × 1, the tilting of the Ge dimers creates an uneven distribution of charge within the dimer, resulting in an electron-rich, nucleophilic “up” atom and an electron-deficient, electrophilic “down” atom. This zwitterionic or acid/base character plays an important role in the reaction of carboxylic acids with the surface.

The large number of similarities between Si(100)-2 × 1 and Ge(100)-2 × 1[18] would lead one to expect that carboxylic acids will form similar surface adducts on both surfaces. Several research groups have previously investigated carboxylic acids on Si(100)-2 × 1 and provide convincing evidence that the majority reaction pathway is O−H dissociation.[20−26] On the

---

(1) Yates, J. T. *Science* **1998**, *279*, 335.
(2) Lopinski, G. P.; Wayner, D. D. M.; Wolkow, R. A. *Nature* **2000**, *406*, 48.
(3) Lin, Z.; Strother, T.; Cai, W.; Cao, X. P.; Smith, L. M.; Hamers, R. J. *Langmuir* **2002**, *18*, 788.
(4) Stewart, M. P.; Buriak, J. M. *Comments Inorg. Chem.* **2002**, *23*, 179.
(5) Guisinger, N. P.; Greene, M. E.; Basu, R.; Baluch, A. S.; Hersam, M. C. *Nano Lett.* **2004**, *4*, 55.
(6) Buriak, J. M. *Chem. Rev.* **2002**, *102*, 1271.
(7) Bent, S. F. *Surf. Sci.* **2002**, *500*, 879.
(8) Filler, M. A.; Bent, S. F. *Prog. Surf. Sci.* **2003**, *73*, 1.
(9) Hovis, J. S.; Liu, H. B.; Hamers, R. J. *J. Phys. Chem. B* **1998**, *102*, 6873.
(10) Kim, A.; Maeng, J. Y.; Lee, J. Y.; Kim, S. *J. Chem. Phys.* **2002**, *117*, 10215.
(11) Wang, G. T.; Mui, C.; Musgrave, C. B.; Bent, S. F. *J. Am. Chem. Soc.* **2002**, *124*, 8990.
(12) Wang, G. T.; Mui, C.; Tannaci, J. F.; Filler, M. A.; Musgrave, C. B.; Bent, S. F. *J. Phys. Chem. B* **2003**, *107*, 4982.
(13) Teague, L. C.; Boland, J. J. *J. Phys. Chem. B* **2003**, *107*, 3820.
(14) Wang, G. T.; Mui, C.; Musgrave, C. B.; Bent, S. F. *J. Phys. Chem. B* **2001**, *105*, 12559.
(15) Develyn, M. P.; Cohen, S. M.; Rouchouze, E.; Yang, Y. L. *J. Chem. Phys.* **1993**, *98*, 3560.
(16) Mui, C.; Bent, S. F.; Musgrave, C. B. *J. Phys. Chem. A* **2000**, *104*, 2457.
(17) Kubby, J. A.; Griffith, J. E.; Becker, R. S.; Vickers, J. S. *Phys. Rev. B* **1987**, *36*, 6079.
(18) Duke, C. B. *Chem. Rev.* **1996**, *96*, 1237.
(19) Zandvliet, H. J. W. *Phys. Rep.* **2003**, *388*, 1.
(20) Tanaka, S.; Onchi, M.; Nishijima, M. *J. Chem. Phys.* **1989**, *91*, 2712.
(21) Sekiguchi, H. I.; Sekiguchi, T. *Surf. Sci.* **1997**, *390*, 214.
(22) Ikeura, H.; Sekiguchi, T. *Surf. Sci.* **1999**, *433−435*, 549.
(23) Bitzer, T.; Alkunshalie, T.; Richardson, N. V. *Surf. Sci.* **1996**, *368*, 202.

10.1021/ja0549502 CCC: $33.50

basis of the observed energy difference of the $\nu$(C═O) and $\nu$(C−O) peaks in their high-resolution electron energy loss spectroscopy (HREELS) data, Tanaka et al. conclude that formic acid forms a monodentate O−H dissociation product on Si(100)-2 × 1 at room temperature. More recently, Bitzer et al.[23] and Lopez et al.[24,25] report an O−H dissociation product on Si(100)-2 × 1 following reaction of benzoic acid and the multifunctional molecules glycine and 4-aminobenzoic acid, respectively. Hwang et al.[26] investigated the reaction of vinyl acetic acid on Si(100)-2 × 1 using low-energy electron diffraction (LEED), X-ray photoelectron spectroscopy (XPS), and synchrotron radiation photoemission spectroscopy (SRPES). These authors also find that the majority product after chemisorption is an O−H dissociation product, although they acknowledge that some minority products may also be present on the surface.

While O−H dissociation is reported to be the majority pathway on Si(100)-2 × 1, the potential still exists for different or additional surface reactions to be observed for acetic acid. We postulate that acetic acid is also capable of reacting through the pathways which have been previously reported for acetone due to the presence of α-CH bonds in both molecules. Researchers report that acetone, a ketone, undergoes a thermodynamically favored α-CH dissociation (“ene”) reaction on the Ge(100)-2 × 1 surface.[14] On Si(100)-2 × 1, it is experimentally observed that the adsorption of acetone yields a wide distribution of surface products, including a [2 + 2] C═O cycloaddition product.[27]

Several studies of the reactions of organics with Si(100)-2 × 1 and Ge(100)-2 × 1 provide confirmation that various interdimer products and interactions are present upon adsorption,[13,28−30] although, to our knowledge, no evidence of interdimer products has been reported for carboxylic acids. Interdimer products are feasible because breaking the weak $\pi$ bonds of two Si or Ge dimers instead of one results in an additional energy cost of only 2−8 kcal/mol on Si[15,16,31−33] or 5−6 kcal/mol on Ge,[15,16] respectively. For certain systems that form [4 + 2] cycloaddition adducts, for example, interdimer bonding is expected to relieve ring strain. For the case of carboxylic acids, infrared evidence presented here points to charge donation from the carbonyl oxygen of the O−H dissociation product to a neighboring surface dimer, creating a bidentate bridging surface structure similar to those observed on various metals.[34,35]

## II. Experimental and Computational Details

Infrared experiments were completed under ultrahigh vacuum conditions (UHV) in a reaction chamber described previously.[36] The base pressure in the chamber is less than $1 \times 10^{-10}$ Torr. The surface was prepared by $Ar^+$ sputtering at room temperature (20 mA emission current, 0.5 keV accelerating voltage, 7−8 $\mu$A sample current) for 20 min followed by annealing to 900 K for 5 min. The design of the tungsten heater in this reactor,[36] combined with the thickness and lateral dimensions of the crystals employed for infrared measurements (19 × 14 × 1 $mm^3$, 45° beveled edges), precludes heating during the sputtering process as well as annealing beyond 900 K. Although the cleaning procedure in this chamber differed from that in our XPS chamber (see following), low-energy electron diffraction (LEED) confirmed that the proper surface reconstruction was achieved, and Auger electron spectroscopy (AES) verified that carbon, oxygen, and nitrogen surface concentrations were undetectable. Infrared spectra were collected in a multiple internal reflection (MIR) geometry by employing a BioRad FTS-60A Fourier transform infrared (FTIR) spectrometer equipped with a liquid nitrogen cooled narrow-band mercury−cadmium−telluride (MCT) detector. The unpolarized beam from the FTIR spectrometer enters the chamber through a $CaF_2$ viewport, is focused onto the beveled edge of a germanium MIR crystal (Umicore), and exits through another $CaF_2$ viewport at a right angle to the first viewport. The beam path is purged by dry, carbon dioxide-filtered air to eliminate the spectral features of $H_2O$ and $CO_2$. The spectral range of the collected infrared data is limited by the absorption of the $CaF_2$ windows, resulting in a low-frequency cutoff of 1100 $cm^{-1}$. We do not show regions above 2100 $cm^{-1}$ because adsorptions in the $\nu$(C−H) and $\nu$(O−H) stretching regions (∼2700−3100 and ∼3400−3700 $cm^{-1}$, respectively) were not intense enough to be observed with our setup. To record infrared spectra of the unreacted molecules, several multilayers were condensed on the sample surface at low temperature. All spectra were corrected for baseline sloping with linear functions between points placed in regions with no spectral features.

X-ray photoelectron studies were carried out in a reactor constructed from stainless steel and equipped with a 220 L/s ion and Ti sublimation combination pump (Perkin-Elmer, TNB-X) as well as a 180 L/s turbomolecular pump (Pfeiffer-Balzers, TPU 180H) in the main chamber. This pumping combination achieves an overall chamber base pressure less than $1 \times 10^{-10}$ Torr as measured by a hot-cathode ionization gauge. The X-ray photoelectron spectrometer consists of a dual anode X-ray source (Specs, XR-50) and a five channeltron hemispherical analyzer (Specs, Phoibos 100). A variable temperature scanning tunneling microscope (STM) (Omicron) is connected to the main chamber via a gate valve and pumped separately by 220 L/s triode ion pump (Varian, 912−7014). The Ge(100) crystal (approximately 3 mm × 10 mm) can be heated resistively and cooled by heat exchange with a liquid nitrogen reservoir in contact with the sample holder through a copper braid.

For X-ray photoelectron experiments, the Ge(100) crystal (0.1−0.39 Ω·cm, p-type, B-doped) was cleaned by $Ar^+$ sputtering at 900 K (20 mA emission current, 1.0 keV accelerating voltage, 12 $\mu$A sample current) for 30 min followed by annealing to 1000 K for 15 min. Following this preparation procedure, carbon, oxygen, and nitrogen levels were below the detection limit of our X-ray spectrometer. STM images confirm a mixed c(4 × 2) and 2 × 1 surface reconstruction following this preparation procedure.[19] Due to interference by the germanium Auger series, it was necessary to record C(1s) and O(1s) photoelectron spectra (250 W = 12.5 kV anode voltage, 20 mA emission current) with the Al and Mg anodes, respectively. The emitted electrons were collected at a takeoff angle of 25°, an acceptance angle of ca. ±5°, and a pass energy of 25 eV. The Ge(3d) photoelectron peak was employed as an internal standard with which to calibrate the energy scale and peak intensity. Shirley baseline subtractions[37] were

---

(24) Lopez, A.; Bitzer, T.; Heller, T.; Richardson, N. V. *Surf. Sci.* **2001**, *480*, 65.
(25) Lopez, A.; Heller, T.; Bitzer, T.; Richardson, N. V. *Chem. Phys.* **2002**, *277*, 1.
(26) Hwang, H.-N.; Baik, J. Y.; An, K.-S.; Lee, S. S.; Kim, Y.; Hwang, C. C.; Kim, B. *J. Phys. Chem. B* **2004**, *108*, 8379.
(27) Armstrong, J. L.; White, J. M.; Langell, M. *J. Vac. Sci. Technol. A* **1997**, *15*, 1146.
(28) Hofer, W. A.; Fisher, A. J.; Bitzer, T.; Rada, T.; Richardson, N. V. *Chem. Phys. Lett.* **2002**, *355*, 347.
(29) Rangan, S.; Kubsky, S.; Gallet, J. J.; Bournel, F.; Le Guen, K.; Dufour, G.; Rochet, F.; Funke, R.; Kneppe, M.; Piaszenski, G.; Kohler, U.; Sirotti, F. *Phys. Rev. B* **2005**, *71*, 125320.
(30) Kim, A.; Filler, M. A.; Kim, S.; Bent, S. F. *J. Am. Chem. Soc.* **2005**, *127*, 6123.
(31) Develyn, M. P.; Yang, Y. M. L.; Sutcu, L. F. *J. Chem. Phys.* **1992**, *96*, 852.
(32) Hofer, U.; Li, L. P.; Heinz, T. F. *Phys. Rev. B* **1992**, *45*, 9485.
(33) Nachtigall, P.; Jordan, K. D.; Sosa, C. *J. Phys. Chem.* **1993**, *97*, 11666.
(34) Weisel, M. D.; Chen, J. G.; Hoffmann, F. M.; Sun, Y. K.; Weinberg, W. H. *J. Chem. Phys.* **1992**, *97*, 9396.
(35) Sim, W. S.; Gardner, P.; King, D. A. *J. Phys. Chem.* **1996**, *100*, 12509.
(36) Mui, C.; Han, J. H.; Wang, G. T.; Musgrave, C. B.; Bent, S. F. *J. Am. Chem. Soc.* **2002**, *124*, 4027.

applied and a chemically realistic number of Voigt components were fit to each photoelectron spectrum. With our spectrometer set at a pass energy of 25 eV, the C(1s) spectrum of ethylene chemisorbed on Ge(100)-2 × 1 shows a single peak centered at 283.7 eV with a fwhm of 1.6 eV, while the O(1s) spectrum of methanol on Ge(100)-2 × 1 reveals a peak at 531.2 eV with a fwhm of nearly 2.0 eV. While all synthetic components within each spectrum were forced to have the same fwhm, the value was allowed to be 1.6 ± 0.2 and 2.0 ± 0.2 eV for the C(1s) and O(1s) photoelectron spectra, respectively.

Acetic acid (99.9%, J.T. Baker), formic acid (99%, Acros), and acetic-$d_3$ acid-*d* (99.5 atom % D, Aldrich) are clear liquids under ambient conditions, and transfer to sample vials was completed under dry air purge. Each compound was purified by several freeze−pump−thaw cycles before exposure to the crystal surface through a variable leak valve and directed doser. Surface exposures are reported in Langmuirs (1 L = $10^{-6}$ Torr•s), and pressures were not corrected for ionization gauge sensitivity. In an effort to minimize reaction of these corrosive acids with the inner walls of the stainless steel gas handling manifold, the compounds were allowed to enter the vacuum chamber within 5 s of filling the lines. Following each surface exposure, the manifold lines were pumped out to less than 20 mTorr before refilling for the following dose. An in situ quadrupole mass spectrometer confirmed the molecular identity and purity of each compound after introduction to either chamber.

Electronic structure calculations were completed with the Gaussian 98 software package[38] using Becke3 Lee−Yang−Parr (B3LYP) three-parameter density functional theory.[39] Previous studies of B3LYP indicate that it provides predictive results for similar systems[12,40,41] and is in good agreement when experimental results are available.[36,42,43] Single dimer $Ge_2Si_7H_{12}$ and double dimer $Ge_4Si_{11}H_{16}$ cluster models were used to model intra- and interdimer surface products, respectively. Only the dimer atoms are modeled as Ge to keep calculations computationally manageable; however, both models are reported to be acceptable to predict reaction products as well as experimental trends.[11,16,36,44] Since the $Ge_4Si_{11}H_{16}$ cluster model is computationally intensive, its use is limited to an investigation of the bidentate structure proposed in the present work. Structures for the one dimer model were fully optimized without geometrical constraints. To minimize aphysical cluster geometries resulting from interdimer adsorbate interactions on the $Ge_4Si_{11}H_{16}$ cluster,[45] the positions of the third and fourth layer Si atoms were fixed in their positions following optimization of an unconstrained $Ge_4Si_{11}H_{16}$ cluster. Geometries of important local minima and transition states on the potential energy surface were calculated with the polarized double-ζ, 6-31G(d) basis set followed by a single point calculation at the 6-31G(d) geometry with the more accurate, triple-ζ, 6-311++G(2df,pd) basis set. Local minima and transition states were verified with frequency calculations of the optimized structure with the 6-31G(d) basis set. All energies were reported without zero-point correction.

## III. Results and Discussion

**A. Density Functional Theory. 1. O−H Dissociation Pathways.** We begin with a discussion of our DFT results for acetic acid. Figure 1 illustrates the two calculated O−H dissociation reaction pathways of acetic acid on Ge(100)-2 × 1. Two different dative-bonded states (a and b), as well as the O−H dissociated product (c) are illustrated in the figure. Discussion of other reaction pathways is deferred until the next section (III.A.2.). The calculations show two possible dative-bonded structures during the chemisorption of acetic acid on Ge(100)-2 × 1. Dative bond formation through the carbonyl oxygen, shown in Figure 1a, is highly exothermic, and this intermediate is predicted to lie 16.5 kcal/mol below the energy level of the reactants. Interestingly, this dative bond is very stable when compared to other carbonyl-containing molecules on Ge(100)-2 × 1. For example, Wang et al. report dative bonds 12.0 and 11.0 kcal/mol below the entrance channel for acetone and ethylvinyl ketone, respectively.[11,14] When the hydroxyl group is rotated away from the dimer (not shown), the binding energy of this dative-bonded state decreases to approximately 6 kcal/mol below the entrance channel. This suggests that roughly 10 kcal/mol of additional stability is gained when the O−C−O bond is aligned over the surface dimer to form a pseudo-six-membered ring stabilized on one side by the Ge⋯O dative bond and on the other by a Ge⋯H hydrogen bond-like interaction, as depicted in Figure 1a. The calculations indicate that this orientation also enables a substantial amount of electron delocalization between the π orbitals of the molecule and the surface.

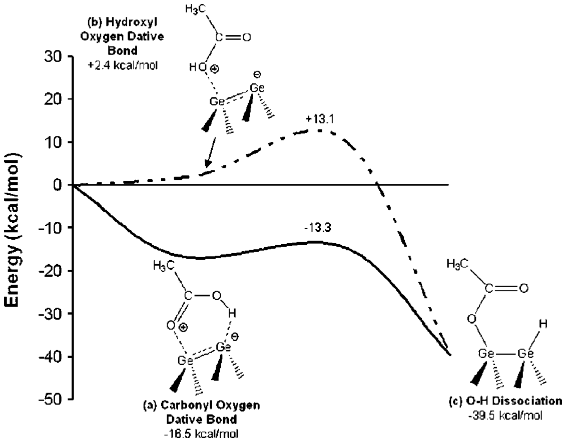

*Figure 1.* Critical points of the O−H dissociation reaction pathways of acetic acid with a $Ge_2Si_7H_{12}$ dimer cluster: (a) carbonyl oxygen dative-bonded state, (b) hydroxyl oxygen dative-bonded state, (c) O−H dissociation product. The O−H dissociation product can be formed either through the carbonyl oxygen dative-bonded state or through a hydroxyl oxygen dative-bonded state.

Following adsorption in this unusually stable carbonyl oxygen dative-bonded state, a small barrier, located 13.3 kcal/mol below the entrance channel, must be surmounted to reach the O−H dissociation product with an overall binding energy of 39.5 kcal/mol (Figure 1c). Of published systems on Ge(100)-2 × 1, only the Diels−Alder product of 1,3-butadiene[16] and the hetero-Diels−Alder cycloaddition product of ethylvinyl ketone[11] possess a comparable or greater thermodynamic stability to the O−H dissociation product of acetic acid on Ge(100). The low activation barrier and stable binding energy suggest that the O−H dissociation pathway should be the dominant surface reaction for acetic acid and other carboxylic acids on Ge(100)-2 × 1.

An O−H dissociation product can also be formed through the hydroxyl oxygen dative-bonded state shown in Figure 1b.

---

(37) Shirley, D. A. *Phys. Rev. B* **1972**, *5*, 4709.

(38) Frisch, M. J.; et al. *Gaussian 98*, revision A.5; Gaussian, Inc.: Pittsburgh, PA, 1998.

(39) Kohn, W.; Sham, L. J. *Phys. Rev.* **1965**, *140*, A1133.

(40) Konecny, R.; Doren, D. J. *Surf. Sci.* **1998**, *417*, 169.

(41) Lu, X.; Lin, M. C. *Int. Rev. Phys. Chem.* **2002**, *21*, 137.

(42) Teplyakov, A. V.; Kong, M. J.; Bent, S. F. *J. Am. Chem. Soc.* **1997**, *119*, 11100.

(43) Zhang, L. H.; Carman, A. J.; Casey, S. M. *J. Phys. Chem. B* **2003**, *107*, 8424.

(44) Filler, M. A.; Mui, C.; Musgrave, C. B.; Bent, S. F. *J. Am. Chem. Soc.* **2003**, *125*, 4928.

(45) Phillips, M. A.; Besley, N. A.; Gill, P. M. W.; Moriarty, P. *Phys. Rev. B* **2003**, *67*.

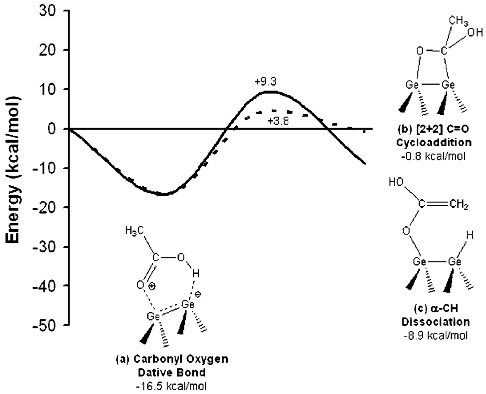

***Figure 2.*** Critical points of the calculated high barrier acetic acid reaction pathways that pass through the carbonyl oxygen dative-bonded precursor state: (a) carbonyl oxygen dative bond, (b) [2 + 2] C═O cycloaddition product, (c) α-CH dissociation ("ene") product.

This pathway was previously identified by Lu and Lin in their theoretical study of formic acid adsorbed on a $Si_9H_{12}$ cluster.[46] Although the dative bond formed through the carbonyl oxygen is unusually stable, the hydroxyl oxygen dative-bonded minimum is calculated to be 2.4 kcal/mol *above* the entrance channel. This interaction between acetic acid and the electrophilic "down" atom of the germanium dimer is energetically unfavorable. Assuming no low barrier pathways are available from the hydroxyl oxygen dative bond, it is expected that adsorbates in this state will rapidly desorb back into the vacuum. It is important to note that, although we searched for an adsorption barrier to the hydroxyl oxygen dative-bonded minimum, none was found. Dissociation of the acidic proton of the hydroxyl group to form the energetically favorable O−H dissociation product requires passage over a high activation barrier, located 13.1 kcal/mol above the entrance channel. This high activation barrier combined with the unstable dative bond indicates that this O−H dissociation pathway is not likely to contribute significantly to the overall surface product distribution.

**2. Other Reaction Pathways.** We now turn our attention to reaction pathways that do not result in the O−H dissociation product. Figures 2 and 3 each display two additional reaction pathways that we have investigated theoretically. We have located two additional pathways that proceed through the carbonyl oxygen dative-bonded state, shown in Figure 2, and two more pathways that occur through the hydroxyl oxygen dative-bonded state, depicted in Figure 3. The α-CH dissociation product, illustrated in Figure 2c, is analogous to the majority product of acetone on Ge(100)-2 × 1.[14] When compared to acetone, the kinetic barrier to formation of the α-CH dissociation product for acetic acid is quite high at 9.3 kcal/mol above the entrance channel. In previous studies, products forming through pathways containing activation barriers of 6−8 kcal/mol above the energy of the reactants have not been observed experimentally.[36,43,44] The final product is also rather unstable at 8.9 kcal/mol below the energy level of the reactants. In contrast, the α-CH dissociation product of acetone was previously calculated to lie approximately 22.8 kcal/mol below the entrance channel.[14] The high barrier and weak binding energy suggest that the α-CH dissociation product will not be observed for acetic acid on Ge(100)-2 × 1. The [2 + 2] C═O cycloaddition pathway (Figure 2b) exhibits a transition state 3.8 kcal/mol above the entrance channel and leads to a product lying just 0.8 kcal/mol below the energy of the isolated reactants. The small binding energy results in a surface product that should rapidly desorb at 310 K,[11,14] and therefore, we also do not expect to experimentally observe the [2 + 2] C═O cycloadduct.

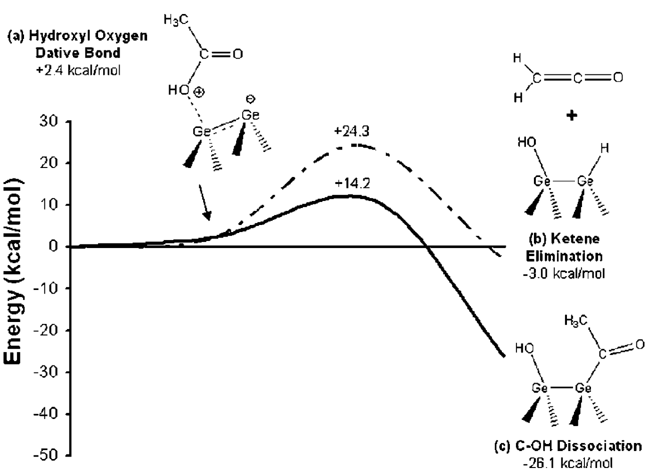

***Figure 3.*** Critical points of the calculated high barrier acetic acid reaction pathways that pass through the hydroxyl oxygen dative-bonded precursor state: (a) hydroxyl oxygen dative bond, (b) ketene elimination product, (c) C−OH dissociation product.

Like the O−H dissociation pathway discussed in section III.A.1., we found two additional pathways which proceed through the hydroxyl oxygen dative-bonded state but possess prohibitively high activation barriers (Figure 3). The ketene elimination product, depicted in Figure 3b, consists of a gaseous ketene molecule as well as a hydroxyl and hydrogen-terminated dimer. The surface adducts resemble those formed by dissociation of a water molecule on Si(100)-2 × 1.[47] The 24.3 kcal/mol activation barrier between the dative bond and the ketene elimination product is high for organics on Ge(100)-2 × 1, and as stated in our previous discussion of activation barriers, the magnitude of this activation barrier will prohibit ketene elimination from proceeding appreciably at room temperature. Finally, the C−OH dissociation pathway also possesses a high activation barrier, calculated to be 14.2 kcal/mol above the entrance channel. However, unlike the ketene elimination product located 3.0 kcal/mol below the entrance channel, we calculate the C−OH dissociation product to lie far below the energy of the reactants at 26.1 kcal/mol (Figure 3c). Despite a thermodynamically favorable end product, the kinetic barrier to formation of the C−OH dissociation product is likely too high for the C−OH dissociation product to contribute to the surface product distribution at room temperature.

**B. Experimental Results. 1. Acetic Acid.** Infrared results from a coverage dependent study of acetic acid adsorbed on Ge(100)-2 × 1 at room temperature and multilayers adsorbed at low temperature are shown in Figure 4a and b, respectively. The key peaks of the multilayer spectrum, appearing at 1697, 1440, 1414, 1360, and 1302 $cm^{-1}$, are in excellent agreement with previously published low-temperature spectra of molecular acetic acid.[48,49] The strong peak at 1697 $cm^{-1}$ is attributed to the $\nu$(C═O) stretching mode. By comparison with Haurie et

---

[46] Lu, X.; Zhang, Q.; Lin, M. C. *Phys. Chem. Chem. Phys.* **2001**, *3*, 2156.

[47] Weldon, M. K.; Stefanov, B. B.; Raghavachari, K.; Chabal, Y. J. *Phys. Rev. Lett.* **1997**, *79*, 2851.

[48] Teragni, P.; Masetti, G.; Zerbi, G. *Chem. Phys.* **1978**, *28*, 55.

[49] Haurie, M.; Novak, A. *J. Chim. Phys.* **1965**, *62*, 146.

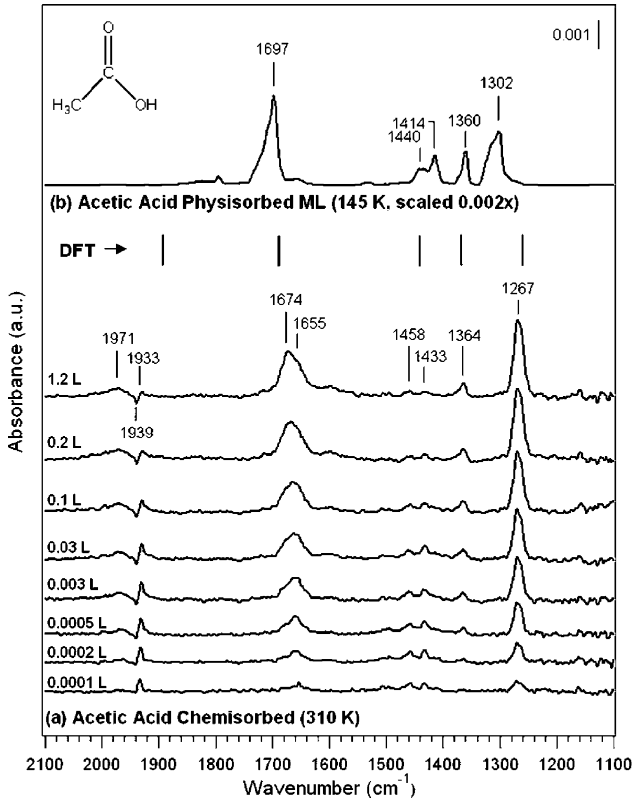

***Figure 4.*** (a) Coverage dependent infrared spectra for the reaction of acetic acid on Ge(100)-2 × 1 at 310 K and (b) acetic acid multilayers adsorbed at 145 K (scaled). Vertical sticks mark the theoretically calculated vibrational frequencies of the O−H dissociation product (scaled by 0.96 for the B3LYP/6-31G* level of theory[52]).

al.,[50] the peaks at 1440 and 1360 cm$^{-1}$ can be assigned to asymmetric and symmetric $\delta(CH_3)$ bending modes, respectively, while the mode at 1414 cm$^{-1}$ is assigned to a $\delta$(OH) bending mode. The intense absorption feature at 1302 cm$^{-1}$ can be attributed to a skeletal stretching vibration with the strongest contribution coming from the C−O single bond.[49,51]

The adsorption of acetic acid as a function of coverage on Ge(100)-2 × 1 at 310 K reveals several interesting spectral features (Figure 4a). For coverages increasing from 0.0001 to 1.2 L, broad $\nu$(Ge−H) and intense $\nu$(C═O) stretching modes are visible at 1971 and 1674/1655 cm$^{-1}$, respectively. The presence of these modes strongly suggests that an O−H dissociation reaction is occurring at 310 K. In addition, the symmetric $\delta(CH_3)$ deformation mode at 1364 cm$^{-1}$ is only slightly shifted from its position in the multilayer. The $\nu$(C−O) skeletal vibration present in the multilayer spectrum at 1302 cm$^{-1}$ appears to have red-shifted to 1267 cm$^{-1}$ in the chemisorbed spectrum. A previous infrared study of the organogermanium compound acetoxygermane ($GeH_3OCOCH_3$) assigns a peak at 1275 cm$^{-1}$ to this skeletal stretching mode, in agreement with the observed shift.[51] The apparent lack of an $\delta$(OH) bending mode in the chemisorbed product, at 1414 cm$^{-1}$ in the multilayer, is also consistent with the O−H dissociation reaction. At a saturation exposure of 1.2 L, the $\nu$(C═O) mode exhibits two distinct vibrational frequencies at 1674 and 1655 cm$^{-1}$ (overall fwhm ≈ 35 cm$^{-1}$). Carbonyl-containing compounds in condensed phases are known to often exhibit split $\nu$(C═O) stretching peaks as a result of subtle conformational differences.[53] Therefore, these distinct absorption modes for acetic acid are attributed to O−H dissociation products in slightly different orientations or conformations. This effect is found for all of the carboxylic acids studied here.

The theoretical spectrum of the O−H dissociation products (shown as sticks in Figure 4) exhibits several similarities to the experimentally obtained chemisorbed spectrum. The major peaks of the calculated spectrum appear at 1890, 1688, 1440, 1366, and 1258 cm$^{-1}$ (scaled by 0.96 for the B3LYP/6-31G* level of theory[52]). The mode at 1258 cm$^{-1}$ is the skeletal mode discussed above, while the peaks at 1366 and 1440 cm$^{-1}$ are due to symmetric and asymmetric methyl bending modes, respectively. The peak at 1688 cm$^{-1}$ is a $\nu$(C═O) carbonyl stretching mode and is only blue-shifted 18 cm$^{-1}$ from the $\nu$(C═O) peak maximum in the room temperature spectrum (Figure 4a).

Two discrepancies exist between the experimental and theoretical spectra which must be addressed. First, although a single peak is calculated to exist at 1440 cm$^{-1}$ for the O−H dissociation product, two weak modes are experimentally observed at 1433 and 1458 cm$^{-1}$. Previous infrared spectra of solid, liquid, and gaseous acetic acid,[49,50,54,55] as well as acetoxygermane,[51] also exhibit only one mode in this spectral region. Interestingly, the peaks at 1433 and 1458 cm$^{-1}$ are strongest at low coverage and significantly attenuate by saturation. Further discussion of the surface structure responsible for these two modes will be deferred until section III.B.2. Second, the calculations also identify a single $\nu$(Ge−H) stretching mode at 1890 cm$^{-1}$. However, following the adsorption of acetic acid on Ge(100)-2 × 1, multiple absorption features are visible above 1900 cm$^{-1}$. This spectral region is significantly more complex than that for acetone[14] or ethylenediamine,[30] which both dissociate hydrogen on Ge(100)-2 × 1. To our knowledge, previous HREELS investigations of carboxylic acid-containing molecules on Si(100)-2 × 1 do not report more than one peak in the $\nu$(Si−H) stretching region.[20,23−25] In the current work, we observe a sharp growth at 1933 cm$^{-1}$ at low coverage, followed by a much broader growth at 1971 cm$^{-1}$ and concomitant appearance of a derivative feature centered at 1939 cm$^{-1}$ as coverage is increased (Figure 4a). Chabal et al. report that the asymmetric and symmetric $\nu$(Ge−H) stretching modes of the Ge(100)-2 × 1:H monohydride surface appear at 1991 and 1979 cm$^{-1}$.[56] Since the broad and sharp peaks in the acetic acid spectrum are separated by 42 cm$^{-1}$, we believe that these two peaks must correspond to two significantly different vibrational modes and not to asymmetric and symmetric stretches of coupled Ge−H bonds. The broad, higher energy mode at 1971 cm$^{-1}$ agrees with literature values for acetone[14] and ethylenediamine[30] dissociated on Ge(100)-2 × 1, and we believe this is due to $\nu$(Ge−H) stretch resulting from the O−H dissociation product. We attribute the 100 cm$^{-1}$ difference between the theoretical and experimental spectra for this mode to cluster effects resulting from the use of a $Ge_2Si_7H_{12}$ single dimer cluster. The sharp, low-energy mode and related derivative

---

(50) Haurie, M.; Novak, A. *Spectrochim. Acta* **1965**, *21*, 1217.
(51) Srivastava, T. N.; Onyszchuk, M. *Can. J. Chem.* **1963**, *41*, 1244.
(52) Wong, M. W. *Chem. Phys. Lett.* **1996**, *256*, 391.
(53) Coleman, W. M., III; Gordon, B. M. *Appl. Spectrosc.* **1987**, *41*, 1169.
(54) Weltner, W. J. *J. Am. Chem. Soc.* **1955**, *77*, 3941.
(55) Wilmshurst, J. K. *J. Chem. Phys.* **1956**, *25*, 1171.
(56) Chabal, Y. J. *Surf. Sci.* **1986**, *168*, 594.

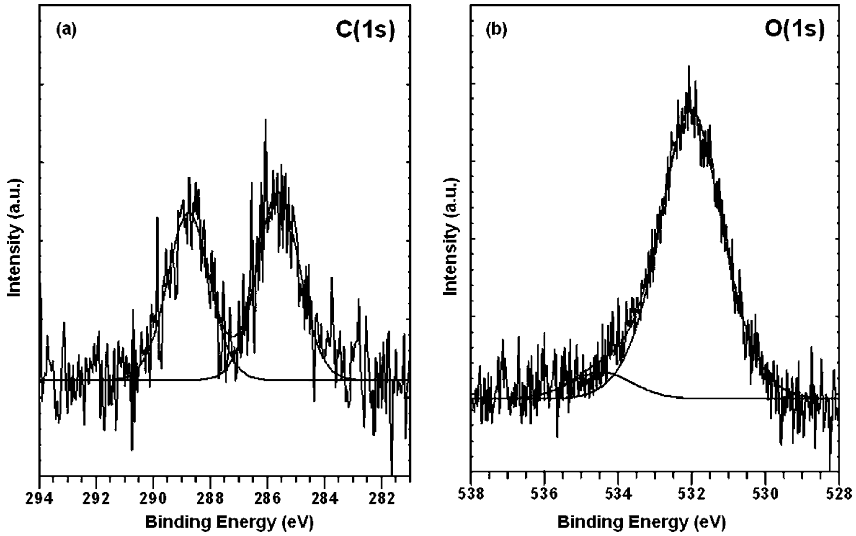

***Figure 5.*** (a) C(1s) and (b) O(1s) photoelectron spectra of a saturation exposure of acetic acid on Ge(100)-2 × 1 at room temperature.

feature appear unrelated to the $\nu$(Ge−H) mode at 1971 cm$^{-1}$, and a full discussion of this mode will be deferred until section III.B.2.

Figure 5 displays the C(1s) and O(1s) X-ray photoelectron data for a saturation exposure of acetic acid on Ge(100)-2 × 1 at room temperature. Two clear peaks of similar intensity centered at 289.0 and 285.8 eV are visible in the C(1s) spectrum, which we attribute to the carbonyl and methyl carbon atoms of the O−H dissociation product, respectively. The O(1s) spectrum shows a large photoelectron peak at 532.0 eV and a weaker component at 534.5 eV, both with a fwhm of 2.0 eV. Although two O(1s) peaks of similar intensity would be expected for the O−H dissociated product, as observed following adsorption of vinyl acetic acid on Si(100)-2 × 1,[26] O(1s) chemical shifts are usually not large and it is possible that two or more unresolved oxygen species are present within the peak at 532.0 eV. The weak, high-binding energy component could result from an inherent asymmetry of photoelectron peaks, as observed for some compounds on the related Si(100)-2 × 1 surface.[57,58] However, a minority species could also exist on the surface, and we will address this possibility shortly. A comparison of the entire C(1s) peak area with that of pyridine, which has five carbons and is reported to saturate at 0.25 ML on Ge(100)-2 × 1,[59] enables us to determine that the surface coverage of acetic acid at saturation is approximately 0.45 ML, or less than one molecule per dimer.

The O−H dissociation product appears to be the majority adduct on the surface. The $\nu$(C−O), $\nu$(C=O), and $\nu$(Ge−H) stretching modes in the infrared spectrum (Figure 4), together with the presence of two C(1s) photoelectron peaks (Figure 5), are consistent with this interpretation. In addition, the O−H dissociation product is the only surface product examined theoretically that possesses all three of the infrared modes listed above. We acknowledge that the spectral data would likely be similar if the α-CH dissociation product was the dominant surface product; however, theoretical calculations (section III.A.) indicate that the branching ratio between the O−H and α-CH dissociation reaction would be on the order of $10^{16}$ at 310 K, precluding observation of the α-CH dissociation product. Similarities between the symmetric $\delta$(CH$_3$) deformation in the chemisorbed and multilayer infrared spectra also suggest that the methyl group remains unchanged following reaction of acetic acid at the surface. As will be discussed later, the adsorption of formic acid on Ge(100)-2 × 1, a molecule without the potential to undergo α-CH dissociation, exhibits vibrational modes that are strikingly similar to those for acetic acid (section III.B.3)

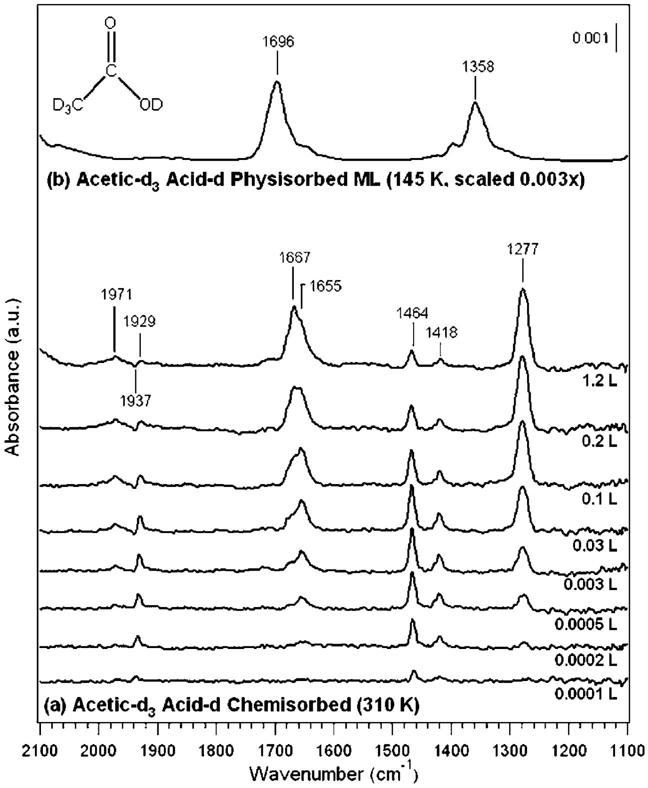

***Figure 6.*** (a) Coverage dependent infrared spectra for the reaction of acetic-$d_3$ acid-*d* on Ge(100)-2 × 1 at 310 K and (b) acetic-$d_3$ acid-*d* multilayers adsorbed at 145 K (scaled).

**2. Acetic-$d_3$ Acid-*d*.** Figure 6a and b shows coverage dependent infrared spectra of the Ge(100)-2 × 1 surface exposed

---

(57) Yeom, H. W.; Baek, S. Y.; Kim, J. W.; Lee, H. S.; Koh, H. *Phys. Rev. B* **2002**, *66*, 115308.

(58) Rochet, F.; Bournel, F.; Gallet, J. J.; Dufour, G.; Lozzi, L.; Sirotti, F. *J. Phys. Chem. B* **2002**, *106*, 4967.

(59) Hong, S.; Cho, Y. E.; Maeng, J. Y.; Kim, S. *J. Phys. Chem. B* **2004**, *108*, 15229.

to acetic-$d_3$ acid-$d$ at room temperature and multilayers physisorbed at 145 K, respectively. The multilayer spectrum contains a $\nu$(C=O) stretching mode at 1696 cm$^{-1}$ and a $\nu$(C−O) skeletal mode at 1358 cm$^{-1}$. These peaks, in addition to higher frequency modes not shown, are in good agreement with previous low-temperature infrared spectra of molecular acetic-$d_3$ acid-$d$.[48,50] The chemisorbed spectrum of acetic-$d_3$ acid-$d$ exhibits many similarities to acetic acid-$d_0$. The peaks at 1667 and 1655 cm$^{-1}$ in the chemisorbed spectrum can be assigned to $\nu$(C=O) carbonyl stretching modes. Again, two distinct $\nu$(C=O) stretching modes can be clearly distinguished, and the convoluted fwhm value is 33 cm$^{-1}$, which is very similar to that in the acetic acid spectrum. The peak at 1277 cm$^{-1}$ closely resembles the peak located at 1267 cm$^{-1}$ in the room temperature acetic acid-$d_0$ spectrum, and it can again be assigned to a skeletal $\nu$(C−O) vibrational stretching mode. The $\delta$($CD_3$) bending modes are significantly red-shifted upon deuterium substitution and are not observed above the 1100 cm$^{-1}$ cutoff of our system. The above data are consistent with the O−D dissociation product as the majority product for the acetic-$d_3$ acid-$d$. However, a peak within the $\nu$(Ge−D) stretch region would also be expected to result from the O−D dissociation for acetic-$d_3$ acid-$d$. Although absorption features are clearly observed at 1418 and 1464 cm$^{-1}$, we do not believe either of these results from such a mode. In addition, the presence of Ge−H bonds on the surface, as exhibited by the broad peak centered at 1971 cm$^{-1}$, is unexpected for the fully deuterated molecule acetic-$d_3$ acid-$d$. We will now address both of these peculiarities in turn.

Coverage dependent spectral changes during the adsorption of acetic-$d_3$ acid-$d$ provide initial clues that the modes at 1418 and 1464 cm$^{-1}$ result from a secondary product on the surface, and not a Ge−D bond. As exposure is gradually increased to 0.03 L, all of the absorption features increase in intensity. Interestingly, as coverage is increased beyond 0.03 L, the modes at 1929, 1464, and 1418 cm$^{-1}$ attenuate, while the modes at 1971, 1667/1655, and 1277 cm$^{-1}$ continue to grow in intensity, suggesting each set of peaks results from different surface adducts. An identical trend is observed for acetic acid-$d_0$ (Figure 4). With increasing coverage, features at 1933, 1458, and 1433 cm$^{-1}$ attenuate, while modes at 1971, 1674/1655, 1364, and 1267 cm$^{-1}$ increase in intensity.

An annealing study of acetic-$d_3$ acid-$d$ confirms that at least two products are present on the surface, and their relative quantities change with temperature. Figure 7 displays infrared data for acetic-$d_3$ acid-$d$ adsorbed at saturation at room temperature (a), followed by annealing to various temperatures (b−e), and a subsequent dose of acetic-$d_3$ acid-$d$ at 310 K (f). At 350 K, the modes near 1655 and 1280 cm$^{-1}$ attenuate in favor of the modes at 1466 and 1419 cm$^{-1}$. A similar, but more pronounced change, occurs upon annealing to 400 K, with the additional increase of a sharp mode at 1931 cm$^{-1}$. By 450 K, all of the modes, except that near 1930 cm$^{-1}$, begin decreasing, and by 500 K, all the modes are attenuating. Subsequent exposure of the annealed surface to 0.1 L acetic-$d_3$ acid-$d$ reforms the original surface products.

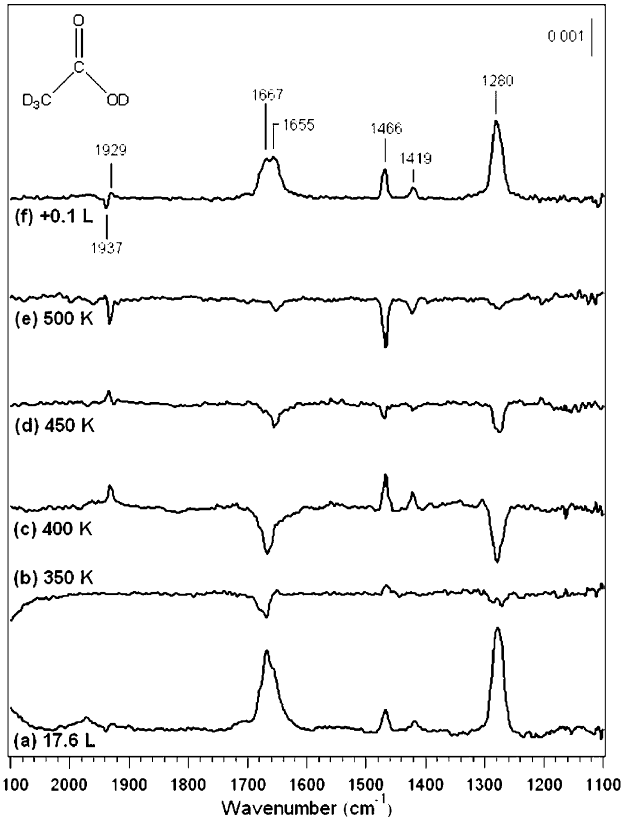

***Figure 7.*** (a) Saturation exposure of acetic-$d_3$ acid-$d$ on Ge(100)-2 × 1 at 310 K followed by annealing for 5 min to (b) 350 K, (c) 400 K, (d) 450 K, (e) 500 K, and (f) a 0.1 L dose of acetic-$d_3$ acid-$d$ at 310 K following the last anneal. Spectrum a is ratioed to the clean surface, while spectra b−f are incrementally ratioed to the previous annealing temperature. All spectra were recorded at 310 K.

From the annealing data, it is clear that at least two different adsorption structures are possible for acetic-$d_3$ acid-$d$. On the basis of the observed spectral changes, it is possible to group the absorption features into two main groups. The first group consists of the modes resulting from the O−H dissociation product near 1667/1655 and 1280 cm$^{-1}$. The second group consists of the peaks at 1929, 1466, and 1419 cm$^{-1}$. To explain the vibrational modes of the second group, we propose the presence of a bidentate bridging structure on the surface, as shown in Figure 8 on a $Ge_4Si_{11}H_{16}$ dimer cluster model. In this type of bridging configuration, both oxygen atoms interact with the surface, creating a O−C−O bond which leads to a substantially red-shifted $\nu$(C=O) stretching frequency. The $\nu_{as}$(O−C−O) and $\nu_s$(O−C−O) infrared absorption modes of acetate and formate bidentate structures created upon the adsorption of acetic acid and formic acid on various metal surfaces, respectively, often fall between 1300 and 1550 cm$^{-1}$,[34,35,60] and are consistent with a bidentate bridging surface structure on Ge(100)-2 × 1. As observed in Figure 7, the increase of the bidentate modes (group 2) at the expense of the O−H dissociation modes (group 1) upon heating points to a pathway where the carbonyl oxygen of the O−H dissociated species can subsequently bond with a nearby surface atom. A saturation coverage of approximately 0.45 ML for acetic acid, while close to one molecule per surface dimer, points to the existence of at least some interdimer products, even at saturation where the bidentate modes are weakest (Figure 4).

DFT calculations identify a stationary point which corresponds to an interdimer bridging bidentate structure on a $Ge_4Si_{11}H_{16}$ cluster model (Figure 8b) and provide additional evidence of the proposed surface structure. The calculated

---

(60) Garcia, A. R.; da Silva, J. L.; Ilharco, L. M. *Surf. Sci.* **1998**, *415*, 183.

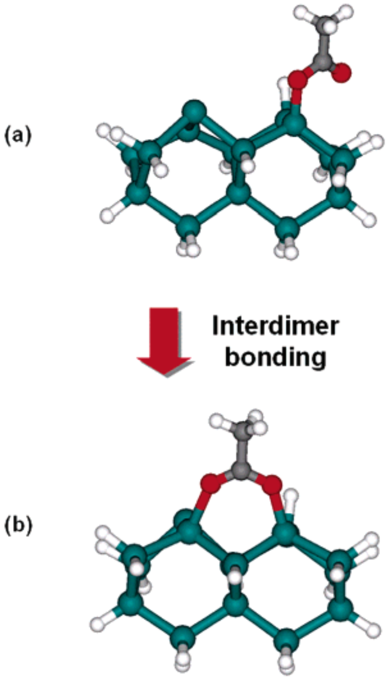

***Figure 8.*** Interdimer bidentate formation calculated on a $Ge_4Si_{11}H_{16}$ dimer cluster model. (a) The O−H dissociation product adjacent to a vacant surface dimer. (b) The oxygen of the surface-bound ester donating charge from the carbonyl oxygen to a neighboring dimer atom.

interdimer species is 2.2 kcal/mol less stable than the O−H dissociation product and exhibits $\nu_{as}$(O−C−O) and $\nu_s$(O−C−O) vibrational frequencies at 1514 and 1322 cm$^{-1}$, respectively. Although the bidentate structure is calculated to be less stable than the O−H dissociation product, the energy difference is well within the error of DFT methods. In addition, the energy likely depends on the type of cluster employed (e.g., $Ge_4Si_{11}H_{16}$ vs $Ge_{15}H_{16}$) as well as the constraints imposed on that cluster. The calculated $\nu_{as}$(O−C−O) and $\nu_s$(O−C−O) vibrational modes of the interdimer species generally agree with the appearance of two vibrational modes in the experimental spectra at 1458/1433 and 1464/1418 cm$^{-1}$ for the bidentate species of acetic acid and acetic-$d_3$ acid-*d*, respectively. However, the calculated $\nu_{as}$(O−C−O) and $\nu_s$(O−C−O) stretching frequencies are separated by 192 cm$^{-1}$, whereas the experimental values are only separated by 25 and 46 cm$^{-1}$ for acetic acid and acetic-$d_3$ acid-*d*, respectively. To explain the large difference between the experimental and theoretical values, we propose that the conformation of the bidentate species differs from that calculated on the $Ge_4Si_{11}H_{16}$ cluster (Figure 8b). It is known that the $\nu_{as}$(O−C−O) and $\nu_s$(O−C−O) frequencies of bidentate surface structures depend heavily on their conformation as well as the surface to which they are bonded.[34,35] Thus, if the surface species exists on a single dimer or between dimers in adjacent rows, rather than between two dimers in the same row, significantly different vibrational frequencies would be expected. While we attempted to calculate bridging bidentate structures in these alternative conformations, the geometry optimizations led to extreme cluster distortions and are therefore not included here. The experimental and theoretical results presented above enable us to conclude that a bidentate structure likely exists on Ge(100)-2 × 1 following adsorption of acetic acid and acetic-$d_3$ acid-*d*; however, additional theoretical studies are required to gain a clearer understanding of its precise conformation.

The infrared coverage and annealing data presented above for acetic acid and acetic-$d_3$ acid-*d* reveal an interconversion between the O−H dissociation product and a bridging bidentate structure. This conversion is observed to have an opposite coverage and temperature dependence. While the bidentate structure converts to the O−H dissociation product upon increasing coverage (Figures 4 and 6), annealing the surface to temperatures near 400 K (Figure 7) causes an increase in the bidentate structure at the expense of the O−H dissociation product. The competition observed as a function of coverage can be understood with the following energetic arguments. As discussed above, the binding energies of the O−H dissociation product and bidentate species shown in Figure 8b are calculated to be approximately the same. However, the initial reaction of acetic acid at the surface to form the O−H dissociation product releases nearly 40 kcal/mol of energy (Figure 1), far more than is gained incrementally by adding a bridging interaction. Therefore, as the number of unreacted surfaces sites decreases, an impinging molecule of acetic acid would be expected to favorably compete with and ultimately dislodge a bridging species, consistent with the observed conversion upon increasing coverage. On the other hand, we believe that the increase in thermal energy during annealing enables conformational changes or surface product ordering that allows formation of additional bidentate surface species.

While we do not completely understand every feature in the spectral region between 1900 and 2000 cm$^{-1}$, several potential sources are now discussed. Although the O−D dissociation reaction appears likely for acetic-$d_3$ acid-*d*, presence of Ge−H bonds on the surface, as exhibited by the broad peak centered at 1971 cm$^{-1}$, is unexpected. The line shape, intensity, and changes with surface exposure of the mode at 1971 cm$^{-1}$ and the derivative centered at 1937 cm$^{-1}$ mirror that of acetic acid-$d_o$ (Figure 4a). We attribute the broad, higher-energy $\nu$(Ge−H) mode to isotopic exchange at the hydroxyl oxygen of acetic-$d_3$ acid-*d* in the stainless steel manifold prior to exposure to the crystal surface. However, the low coverage peak near 1930 cm$^{-1}$, which exhibits derivative behavior as coverage increases, is likely related to the same mode observed at 1933 cm$^{-1}$ in the case of acetic acid-$d_o$, and probably does not result from a $\nu$(Ge−H) mode. We propose the following two explanations for the appearance of this feature. The peak could result from a yet unknown vibration of a bidentate bridging surface structure, although we are unable to make a definitive assignment based on the literature or theory. The potential also exists for defect or thermally induced decomposition processes to form a new minority product on the surface. In the annealing study discussed above (Figure 7), the growth of the mode at 1929 cm$^{-1}$ does not completely correlate with the other peaks in the bidentate group. For example, this mode increases in intensity at 450 K (Figure 7d), while every other mode attenuates. We speculate that the formation of carbonyl monoxide bonded to the Ge(100)-2 × 1 surface could be a potential decomposition product, and reactions that produce carbon monoxide on metal surfaces have long been studied.[35] Reports in the organometallic literature of Ge−C≡O-type bonds, or germanium carbonyls,[61,62]

---

(61) Zhang, L.; Dong, J.; Zhou, M. *J. Chem. Phys.* **2000**, *113*, 8700.

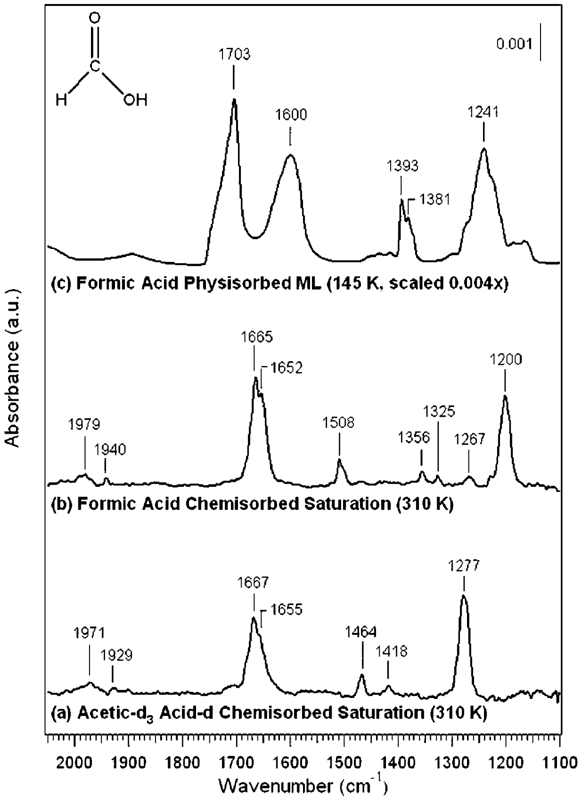

***Figure 9.*** (a) Acetic-$d_3$ acid-*d* saturation exposure on Ge(100)-2 × 1 at 310 K, (b) formic acid saturation exposure on Ge(100)-2 × 1 at 310 K, and formic acid multilayers adsorbed at 145 K (scaled).

indicate that the C≡O bond of these species falls in the low 1900 $\mathrm{cm}^{-1}$ region, in excellent agreement with the peaks at 1933 and 1929 $\mathrm{cm}^{-1}$ following adsorption of acetic acid and acetic-$d_3$ acid-*d*, respectively, on Ge(100)-2 × 1.

We are unable to explain the presence of the negative derivatives observed at the high energy side of the peaks at 1933 and 1929 $\mathrm{cm}^{-1}$ for acetic acid and acetic-$d_3$ acid-*d*, respectively (Figures 4a and 6a). Similar derivatives have been reported near 2100 $\mathrm{cm}^{-1}$ following adsorption on Si(100)-2 × 1[63] and are usually attributed to water previously dissociated on the surface. Since the sticking probability of water on Ge(100)-2 × 1 is considerably less than that on Si(100)-2 × 1,[64] we do not believe the derivative results from preadsorbed water. Furthermore, except for the carboxylic acids studied in the present work, we do not observe derivative behavior in this spectral region for any other compounds adsorbed on Ge(100)-2 × 1. Additional experimentation may be necessary to identify the source of this derivative feature.

**3. Formic Acid.** Formic acid was investigated to ascertain the generality of the O−H dissociation reaction for carboxylic acids on Ge(100)-2 × 1 as well as to further investigate possible bidentate bridging surface structures. Figure 9b and c shows the infrared spectra of formic acid adsorbed on Ge(100)-2 × 1 at 310 K and formic acid multilayers condensed at low temperature, respectively. The chemisorption spectrum of acetic-$d_3$ acid-*d* on Ge(100)-2 × 1 is also included in Figure 9a for reference. Strong peaks appearing in the multilayer spectrum at 1703, 1600, 1393, 1381, and 1241 $\mathrm{cm}^{-1}$ are in excellent agreement with spectra of crystalline formic acid.[65] Two large $\nu$(C═O) stretching modes observed at 1703 and 1600 $\mathrm{cm}^{-1}$ in the multilayer result from individual formic acid molecules forming chains through hydrogen bonding interactions between the hydroxyl hydrogen of one molecule and the carbonyl group of an adjacent molecule. The formation of these molecular chains results in two $\nu$(C═O) stretching modes that are separated by approximately 100 $\mathrm{cm}^{-1}$. Millikan and Pitzer, who performed infrared studies on monomeric, dimeric, and crystalline formic acid, suggest that the higher frequency mode results from out-of-phase stretching, while the lower mode is the result of in-phase stretching.[65] The peaks centered at 1393/1381 and 1240 $\mathrm{cm}^{-1}$ are attributed to $\delta$(C−H) bending and $\nu$(C−O) stretching modes, respectively.

Although the multilayer spectra of acetic-$d_3$ acid-*d* (Figure 6b) and formic acid (Figure 9c) are quite different, the chemisorbed infrared spectra display some striking similarities. The presence of $\nu$(Ge−H), $\nu$(C═O), and $\nu$(C−O) modes at 1979, 1665/1652, and 1200 $\mathrm{cm}^{-1}$, respectively, strongly suggests that formic acid also undergoes an O−H dissociation reaction on Ge(100)-2 × 1. Since no α-CH bonds are present in formic acid, the spectral similarities also provide additional evidence that the α-CH dissociation pathway is not active for acetic acid and acetic-$d_3$ acid-*d*. The appearance of the $\nu$(C−O) mode at 1200 $\mathrm{cm}^{-1}$, red-shifted 77 $\mathrm{cm}^{-1}$ from its position for acetic-$d_3$ acid-*d*, is consistent with a previous spectroscopic study of germyl formate ($HCOOGeH_3$), which assigns peaks near 1210 $\mathrm{cm}^{-1}$ to the $\nu$(C−O) stretching mode.[66] The two peaks again present in the $\nu$(Ge−H) stretching region at 1979 and 1940 $\mathrm{cm}^{-1}$ are assigned in a fashion similar to those for acetic acid and acetic-$d_3$ acid-*d* (see section III.B.2.). Furthermore, the doublet at 1665 and 1652 $\mathrm{cm}^{-1}$ is split by 12 $\mathrm{cm}^{-1}$; the width of these convoluted peaks (fwhm ≈ 29 $\mathrm{cm}^{-1}$) is comparable to the analogous peaks in the spectra of acetic acid and acetic-$d_3$ acid-*d*. As described above, this splitting suggests that the carbonyl bond of the O−H dissociation product is easily perturbed by conformational changes or intermolecular interactions.

An absorption feature which does not correlate with peaks in the multilayer can be clearly observed at 1508 $\mathrm{cm}^{-1}$. Interestingly, this peak falls in the same spectral region as the peaks at 1458/1433 $\mathrm{cm}^{-1}$ and 1464/1418 $\mathrm{cm}^{-1}$ for acetic acid (Figure 4a) and acetic-$d_3$ acid-*d* (Figure 6a), respectively, which were previously assigned to bidentate bridging surface structures (section III.B.2.). This is strong evidence that some formic acid O−H dissociation product can also form bridging structures similar to those for acetic acid and acetic-$d_3$ acid-*d*. The blue-shift of the bidentate vibrational frequency by approximately 50 $\mathrm{cm}^{-1}$ from acetic acid/acetic-$d_3$ acid-*d* to formic acid can be explained by the presence of the lighter hydrogen atom instead of a methyl group at the carbonyl carbon of the bidentate bridging structure.

**4. Comparison with Si(100)-2 × 1.** As outlined section I, several researchers have investigated the adsorption of carboxylic acids on Si(100)-2 × 1 with a variety of experimental techniques.[20−26] The identification of the O−H dis-

---

(62) Feltrin, A.; Cesaro, S. N.; Ramondo, F. *Vib. Spectrosc.* **1996**, *10*, 139.
(63) Mui, C.; Wang, G. T.; Bent, S. F.; Musgrave, C. B. *J. Chem. Phys.* **2001**, *114*, 10170.
(64) Mui, C.; Senosiain, J. P.; Musgrave, C. B. *Langmuir* **2004**, *20*, 7604.
(65) Millikan, R.; Pitzer, K. *J. Am. Chem. Soc.* **1958**, *80*, 3515.
(66) Angus, P. C.; Stobart, S. R. *J. Chem. Soc., Dalton* **1975**, 2342.

sociation product for acetic acid, acetic-$d_3$ acid-*d*, and formic acid in the present work is consistent with previous results on Si(100)-2 × 1. However, while a bidentate bridging configuration is observed here, no previous study on clean Si(100)-2 × 1 reported evidence of a similar structure. Although the strength of the Si−O bond would lead one to expect that the bidentate species is energetically more favorable on Si-(100)-2 × 1 than on Ge(100)-2 × 1, the use of EELS rather than IR may have limited the ability to resolve the features associated with these products. Furthermore, since many of the Si(100)-2 × 1 experiments were carried out at moderate to high surface exposure, where the bidentate vibrational modes observed in the present work are weakest (Figures 4 and 6), the concentration of the bidentate structure is expected to be at a minimum and difficult to detect. This is consistent with our XPS data recorded at saturation exposure (Figure 5), where bidentate features cannot be resolved.

## IV. Conclusions

We have studied the reactions of a series of carboxylic acids, including acetic acid, acetic-$d_3$ acid-*d*, and formic acid, on the Ge(100)-2 × 1 surface using a combination of experimental and theoretical techniques. Infrared and photoelectron experimental data provide substantial evidence that carboxylic acids undergo O−H dissociation reactions at 310 K, and DFT calculations for acetic acid on a single dimer cluster model indicate that this product is both kinetically and thermodynamically favored. Unexpected vibrational modes appearing between 1400 and 1525 $\mathrm{cm}^{-1}$ for all of the carboxylic acids studied here likely result from the formation of bidentate bridging surface structures similar to those reported widely on metals.

Carboxylic acids are found to be useful for functionalizing group IV semiconductor surfaces due to the low kinetic barriers and stable surface moieties of the O−H dissociation product. Previously, carboxylic acids have been used in multifunctional molecules to leave unreacted amines[24,25] and alkenes[26] protruding from the Si(100)-2 × 1 surface, and this work suggests that similar techniques could be employed on Ge(100)-2 × 1.

**Acknowledgment.** This work was supported by the National Science Foundation (CHE 0245260). M.A.F. thanks the National Science Foundation for support in the form of a Graduate Research Fellowship. J.A.V. would like to acknowledge funding in the form of an AVS undergraduate research award. A.J.K. acknowledges support from the Stanford President's Scholar Program and the Merck Award for Student Research. Scientific discussions with Prof. Charles B. Musgrave and Ansoon Kim were helpful and enjoyable.

**Supporting Information Available:** Complete ref 38. This material is available free of charge via the Internet at http://pubs.acs.org.

JA0549502